Surface characterization of plasma-modified carbon fiber: correlation between surface chemistry and morphology of the single strand

D Gravis, S Moisan, Fabienne Poncin-Epaillard

Surface characterization of plasma-modified carbon fiber: correlation between surface chemistry and morphology of the single strand.

D. Gravis[1,2)], S. Moisan[2)], F. Poncin-Epaillard[1,*)]

1) Le Mans Université - CNRS n°6283, Institut des Molécules et Matériaux du Mans, Avenue Olivier Messiaen, 72085 Le Mans, France
2) IRT Jules Verne, Chemin du Chaffault, 44340 Bouguenais, France

*: corresponding author: fabienne.poncin-epaillard@univ-lemans.fr

Keywords: carbon fiber; cold plasma; surface functionalization; wettability; surface physico-chemistry; Raman spectroscopy.

Surfaces and Interfaces 21 (2020) 100731

Abstract:

To prepare cohesive polymeric composite, plasma-modified carbon fibers (CF) were prepared. Among the different strategies to modify the CF surface, the plasma functionalization, a promising eco-process, induces both chemical and topographic modifications of the CF surface. Surface characterization of such material composed of several thousands of single strands requires specific analyzes well suited for both single strand or fiber samples. The wettability measurement of modified strand or fiber thanks to the simple contact angle measure is unobvious. Therefore, their wetting profiles in different liquid probes were captured to determine the exact surface free energy of plasma-modified CF with a remarkable precision. Furthermore, the obtained results were correlated with more conventional chemical and morphological surface analyses. The increase of surface free energy was linked to the appearance of acidic (COO) and ether (C-O-C) groups on plasma-oxidized CF. However, the O_2 plasma-treatment showed a limited improvement of CF surface properties, due to their excessive oxidation altering their crystalline properties.

1. Introduction

For the last decades, carbon-based materials like carbon nanotubes (CNT), carbon fibers (CF) or the less common fullerene and graphene gain more interest as reinforcing materials, especially in polymer composites. These materials are endowed with excellent mechanical properties and good electrical conductivity applied in polymer composites field [1]. However, the CF chemical inertia makes their industrial usability less practical, as their compatibility with most polymer matrices is relatively low [1-3]. Therefore, the CF surface must undergo several

treatments preserving the bulk properties in to improve the CF-polymer matrix compatibility and to ensure the cohesion of the overall polymer composite [4]. Among the different approaches to modify the CF surface, one of them deals with its coating, so-called CF-sizing to create an interphase between CF and polymer matrix. The CF is coated through the grafting of polymer chain [5,6], the whiskerization process [7] or the plasma-polymerization [6-9]. Besides these treatments, oxidative ones aim to modify the CF surface chemistry to increase its compatibility with the polymer matrix, while avoiding surface deposition. Most of them involve the CF immersion in a liquid phase to simultaneously eliminate any non-adherent layers and oxidize their surface [1,10,11]. However, due to toxicity issues of these liquid processes, dry-phase technologies are more and more preconized while ensuring good surface properties. In oxidative dry-phase process, the gaseous atmosphere is composed of air, dioxygen or gases containing oxygen atoms such as ozone and carbon dioxide, heated at temperatures ranging from 400 to 1500 °C. However, these thermal processes induce surface alteration of the CF, and as a consequence its mechanical properties failure [12] even if the addition of metallic catalyst little reduces the atmosphere temperature range [13].

Hence, the cold plasma-functionalization is a successful process, as the CF surface is exposed to a reactive medium which induces a chemical surface modification with a limited topography alteration [1,14-18] issued from various plasma phases like argon [19], dioxygen [20], dinitrogen [10] and their mixture [21]. Evidence of the topographic alteration is given by scanning electron microscopy (SEM) while the incorporation of new surface functional groups is highlighted by X-Ray photoelectron spectroscopy (XPS). Such characterizations are typically driven by the composite application and only few papers aim to show the modification impact on the physico-chemistry of the CF surface, and furthermore on the crystalline modification that could be induced by such dry-phase processes [22,23].

In this study, the surface free energy (SFE) of the several plasma-functionalized CF single strands is determined thanks to an innovative reliable and accurate method of their wetting profiles when dipped in different liquid probes. Comparison with other characterizations (XPS, Raman spectroscopies, SEM) shows that the observed SFE dependence on plasma-grafted chemical groups is strictly unrelated to this surface functionalization but is also correlated to the strand crystallinity as measured by Raman spectroscopy.

2. Materials and methods

2.1 Materials and sample preparation

Single strands of commercial available carbon fiber CF (ex-PAN T300 from Toray composed of 12000 single strands obtained after polyacrylonitrile carbonization) were plasma-treated. Single strands mean diameter was measured around 6.7 ± 0.2 µm. The commercial carbon fibers are often sized. Its goal is broadly to preserve the fiber before impregnation into the polymer matrix and to produce a layer which will constitute an interface between the fiber and the matrix. In most of the cases, the sizing is carried out by depositing a layer of epoxy resin. The unsizing step was performed as follows: carbon fibers were dipped in dichloromethane for 24 h at room temperature, then were rinsed in acetone and ethanol before drying. Samples of 5 to 15 cm of the carbon fibers were then cut before the plasma-treatment.

2.2 Plasma surface treatments

Plasma treatment of single CF strand was performed in a capacitive radio-frequency (RF, 13.56 MHz) plasma reactor. The low pressure is maintained thanks to a turbomolecular

pump (Alcatel ATP-80) coupled with a primary rotary pump. Typical residual pressures are maintained between 10^{-3} and 10^{-2} Pa, while the working pressure is measured around 1 Pa with a capacitive-penning pressure gauge (Alcatel ACC 1009). The glow discharge is sustained between two parallel electrodes separated by a fixed distance of 12 cm, and powered with a Caesar RF generator (Advanced Energy), with powers ranging from 5 to 100 W and durations from 1 to 10 min. Reflected power was kept minimum thanks to RF matchbox (Advanced Energy). Plasma discharges were performed in continuous wave (CW) in different gases: argon (99.99 %), dioxygen (99.5 %), dinitrogen (99.8 %) at constant flow rates of 10 sccm, and in vapor of pure water. For the latter, as the flow rate of water vapor is uncontrolled, H_2O content in the chamber was fixed with a constant working pressure of 2 Pa, equivalent as that obtained for molecular gas pressures.

CF sample was held on a homemade fiber holder that stretched the fiber under a tension of around 1 N on stainless steel vertical poles. The poles' length was fixed to place the fiber parallel to the electrodes, and at a distance of 6 cm from each of the electrodes. The poles were stuck on an ABS plate isolating the poles from the electric field and keeping the CF under floating potential.

2.3 Surface characterization

Wettability and surface free energy

The surface physico-chemistry of the plasma-treated single strand and its dependence on plasma parameters was followed by singular wettability measures. Single strand vertically hung on an aluminum holder was dipped in sampling liquids, either polar such as the ethylene glycol (EG) or apolar as the n-hexadecane (HD). Dispersive and polar surface tension components of both liquids are reported in Table 1.

Table 1 polar (γ_p) and dispersive (γ_d) components of ethylene glycol (EG) and hexadecane (HD)

	γ_p (mJ/m²)	γ_d (mJ/m²)
EG	19.0	29.3
HD	0	24.7

Transparent tank was completely filled with the sampling liquid to ensure a flat surface and to avoid the liquid meniscus appearance. The wetting profile of the dipped strand was recorded in static mode thanks to the goniometer Krüss G10 DSA100.

The surface energy was determined by the Owens-Wendt method [24], by calculating the contact angle of both liquids on the vertical CF strand. To calculate the corresponding contact angle, Young-Laplace equation (eq 1) was solved for a wetting profile on vertical solid plane as described by Arts *et al*. [25]. Coordinates (*x; y*) of the profile were measured on the wetting meniscus picture thanks to the software ImageJ Fig. 1a. The (*x; y*) coordinates are *x*, the lateral distance from the CF strand, and y, the profile height at the corresponding *x* position. The profile height is measured from the planar liquid-air interface at (∞, 0). To solve such an equation, two other data must be taken into account: the capillary rise *h* at (*x; y*) ≡ (0; *h*), and the capillary length l_c, which stands for the distance from the CF strand at *y* almost equal to 0: (*x; y*) ≡ (l_c;0).

$$\frac{x}{l_c} = \operatorname{arccosh}\left(\frac{2l_c}{y}\right) - \operatorname{arccosh}\left(\frac{2l_c}{h}\right) + \sqrt{4 - \frac{h^2}{l_c^2}} - \sqrt{4 - \frac{y^2}{l_c^2}} \qquad \text{(eq 1)}$$

Fig. 1b shows a good agreement between the fit of equation (1) and the measured values (*x*; *y*). Then, the contact angle (θ) of both liquids is calculated from the following equation (2) and the extracted values of *h* and l_c issued from the profile curve.

$$\theta = \arcsin\left(1 - \frac{h^2}{2l_c^2}\right) \qquad \text{(eq 2)}$$

The contact angles of HD and EG then allow to calculate the surface free energy of the CF strand and its respective polar and dispersive components.

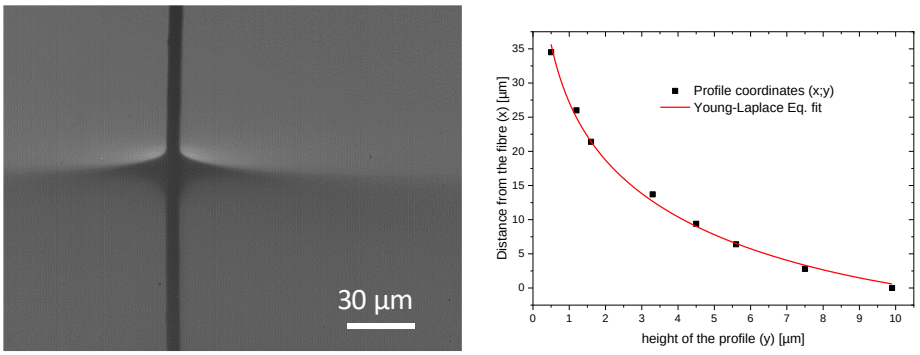

a) b)

Figure 1 wetting profile of the pristine single CF strand immersed in hexadecane (a); plotted profile as measured on the picture (dots) and the corresponding Young-Laplace fitting (line) (b). For easier fitting purpose, coordinates axes are shifted to the right.

Chemical analysis

The XPS analyses were performed with an X-ray Photoelectron Spectrometer Axis Nova (Kratos Analytical). The X-ray radiation was produced by an Al K_α monochromatic source. Pass energies of 80 eV (1eV step) was used for low resolution spectra, while 20 eV (0.1 eV step) pass energy was used for the high-resolution spectra. 10 scans for each high-resolution spectrum of the XPS main C 1s peaks were recorded on at least two spots along the plasma-treated fiber (1 cm-length samples) while a sole scan was only performed for each low resolution spectra. No neutralization was needed for the samples. The calibration was done with the main component of the C1s peak, assigned to the value of 284.7 eV [26]. The results' analysis was performed using Casa XPS software by fitting the main peaks with a Gaussian/Lorentzian shape.

Raman spectroscopy

Raman spectra were gathered thanks to a Horiba Xplora Raman spectrometer built on a confocal microscope Olympus BX41. The green (λ = 532 nm) laser was focalized on single CF strand with a x100 objective. Spectra acquisition was performed in the spectral range 500 to 2000 cm^{-1} at fixed laser power around 5 mW. Scan numbers and durations were kept minimal

to avoid sample destruction, respectively < 10 and < 40 s. The dispersive system consists of a network with 600 strokes/mm.

Scanning electron microscopy

The SEM analyzed run on a Jeol JSM 6510 LV SEM (tungsten filament) microscope, was performed without any sample preparation as CF is semi-conductor but under mild conditions (35 µm spot size and acceleration voltage of 10 keV) avoiding degradation of the strand surface.

3. Results and discussion

3.1 Dependence of the plasma-modified strand wettability on its surface chemistry.

The wettability measure of the fiber bundle or on a single strand is generally performed on bigger and flatter contact surface prepared from compressed fibers or similar material pellet as vitreous carbon [27]. The exact wetting value can be achieved by immersing the material in a liquid probe. However, such a measure induces the wetting profile with capillary length and rise on the same scale of CF dimension (usually ≤ 10 µm) [24,25]. To minimize such a side phenomenon, the measurement was applied to a single strand and viscous liquid probes (HD, η_{HD} = 3.03 mPa.s and EG, η_{EG} = 16.06 mPa.s at 25 °C). Indeed, the capillary rise and length of a too low viscous liquid such as water strongly depend on the surface topography of CF single strand and may cause successively its wetting and dewetting. This issue is absolutely critical as the wetting experiment switches from a static mode to a dynamic mode. HD and EG were accordingly chosen to prevent significant dynamic wetting and to reduce the scattering of the h and l_c measures and consequently of the calculated contact angles (Θ) and exact surface

free energy (SFE). However, several experimental precautions on the profile measurement and subsequent fitting have to be taken into account (Fig. 2):

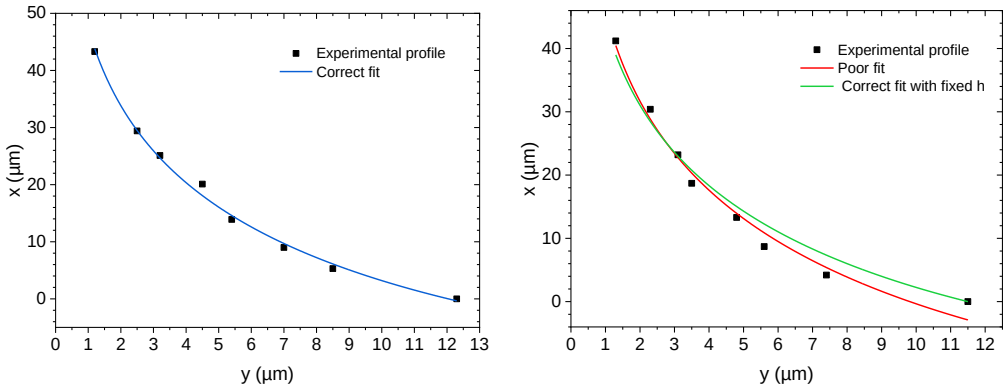

Figure 2 Wetting profiles of the pristine CF strand in HD. (a): profile with a correct fit. (b): the wetting profile induces divergent fitting (red curve), fixing the measured height improves the fitted values (green).

In Fig. 2, depending on analyzed samples, different responses of the fitting iterations are observed. In some cases, the measured profile offers a proper fit even if the parameters of the Young-Laplace equation (eq 1) are varied without any constraint (Fig. 2a) especially for the height (h) values (y = h for x = 0) since h is almost equal to that one measured on the profile. In other cases, a significant deviation from the exact height value with a divergent fitting (Fig. 2b, red curve) is noticed. But, if h values are fixed, a correct fitting ($R^2 \geq 98$ % (Fig. 2b, blue curve) is obtained. A correct fit allows to calculate l_c. It has been also noted that a diverging fitting always induces a bigger variation for h than for l_c. These measurement issues can be caused by the small size of samples, emphasized by a possible too low resolution of the optical lens reducing the measurement accuracy. Thus, to avoid this discrepancy, the h value directly measured on the profile image was injected in the fitting allowing the l_c calculation for a given and measured h. Lowering the freedom degree of the fit parameters induces quite good results with low fitting standard variations for each gathered profiles ($R^2 \geq 95$ %).

The repeatability of the measure (5 conducted with a new pristine CF single strand, in both liquid probes) was also verified (**Erreur ! Source du renvoi introuvable.**).

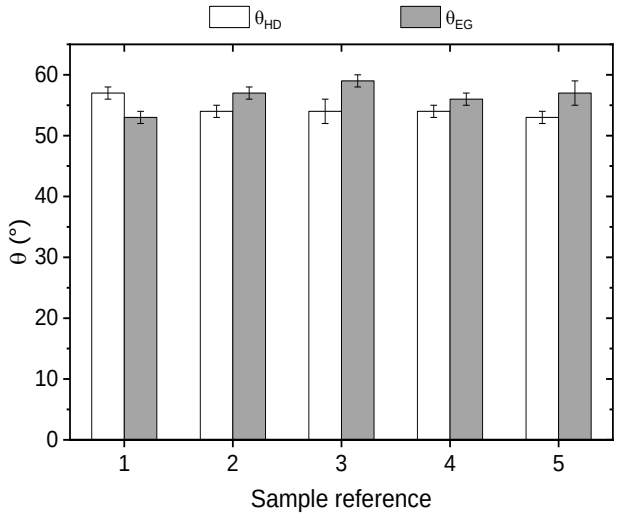

Figure 3 Repeatability of the measurement of HD and EG contact angles for pristine single CF strand referenced as n°1-5.

The contact angles are obtained from eq 2, l_c and h are calculated from the Young-Laplace equation profile fitting. Thus, each reported standard deviation of contact angle is derivative from its corresponding standard deviation of wetting profile fitting. Fig. 3 shows that all Θ of both liquids for untreated single CF strand are comprised between 53 and 59 °. As the fitting itself was conducted with good accuracy, these observed variations in the CA for different pristine strands are significant and can be explained by the dispersion in the single CF strand diameter (6.7 ± 0.2 µm), as well as the inhomogeneity of surface chemistry and topography. This low Θ dispersion induces high standard deviations of SFE values. Indeed, the SFE of the pristine strand and its two dispersive and polar components (γ_d and γ_p) are respectively 27 ± 5 mJ/m², 17 ± 3 mJ/m² and 10 ± 4 mJ/m² with a relative error on γ around 20 %. This SFE deviation is assigned to heterogeneous surface properties of the single CF strands themselves.

Furthermore, this surface energy determination was applied for plasma-modified CF (Fig. 4). The surface free energy of treated CF remains constant whatever the plasma conditions, considering the high relative errors due to dispersion of the measurements.

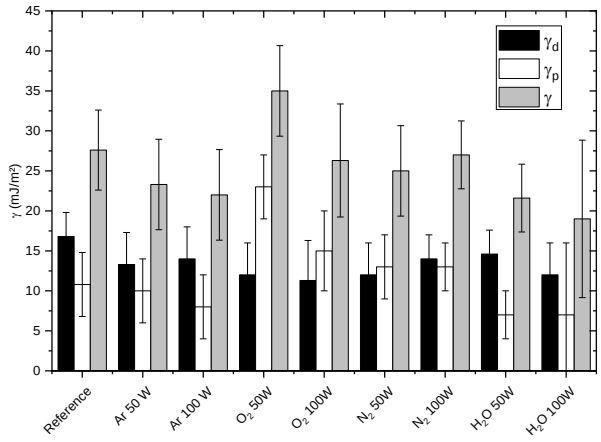

Figure 4 Surface free energy (γ) and its polar (γ_p) and dispersive (γ_d) components of the single CF strand for different gases and applied powers with a fixed exposure time (5 min).

Compared to the surface free energy (γ, γ_d and γ_p) of pristine strand respectively 27 ± 5 mJ/m²,17 ± 3 mJ/m² and 10 ± 4 mJ/m²; the SFE of treated samples does not seem to significantly vary, and remains around values of 27 mJ/m² within standard deviation around 5 mJ/m² whatever the chosen plasma conditions. However, the dioxygen plasma initiated at 50 W discharge power seems to be more efficient; this is explained by the high atomic oxygen reactivity that leads to surface functionalization and even degradation as observed under higher discharge power (100 W). In the former case, the polar component γ_p significantly increases up to 23 ± 4 mJ/m², while its decrease is observed for high-power dioxygen treatment (100 W) and water vapour, argon and it is assigned to an excessive reaction of active species present in the plasma that induces the surface etching of the carbon fiber [17,27,28]. The formed species on the CF surface could also be less stable, react with the environment and then age [27]. The dispersive component γ_d remains around values of 15 mJ/m² and appears to be independent on the treatment parameters. Finally, in the case of dinitrogen treatments, almost no variations are

noted. The still low SFE indicates that the dinitrogen plasma is less efficient to provide surface functionality or degradation, or contributes less to surface polarity.

To highlight the CF chemical modification, low resolution XPS surveys were recorded for CF treated in similar conditions as presented in Figure 4. From this analysis, the elemental composition of each sample was determined (Fig. 5).

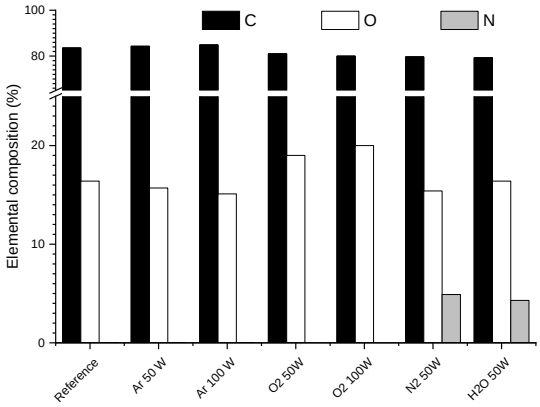

Figure 5 Elemental composition of the untreated and plasma-treated CF for different gases and applied powers with a fixed exposure time (5 min).

The atomic oxygen surface concentration of the pristine material is higher than that one previously reported in [22,29,30], 16.4 % against 10 % or less reflected the pristine CF oxidation during its processing or its aging prior the plasma treatment. When applied an Ar, N_2 or H_2O plasma on CF, the oxygen content remains quite constant around 15.0 % whatever the plasma parameters. Besides, with water and dinitrogen plasma, atomic nitrogen is added to the surface whose concentration is respectively 4.3 and 4.9 %. From this graph, it appears that the Ar plasma-treatment induces less functionalization with almost no oxygen grafting, even more without any post-oxidation and no nitrogen incorporation as also noticed in [19,22]. In addition of the observed decrease of the SFE (Fig. 4), one may conclude that such a modification mostly induces effective etching of the CF surface through removal of the native oxygen-containing groups [31]. The nitrogen atoms grafted on the CF after N_2 plasma-modification therefore lead to the increase of the SFE observed for the treatment (Fig. 4) [1,3,29]. The nitrogen

incorporation in water plasma-functionalized CF is explained by the high solubility of atmospheric dinitrogen in pure water; nevertheless, pure water plasma is not energetic enough to induce an effective modification of the surface chemistry. Lastly, only dioxygen plasma treatment induces a significant increase in the atomic oxygen concentration, up to 19.0 and 20.0 % for discharge powers of 50 and 100 W respectively. The corresponding XPS high resolution spectra of CF are shown in Figure .

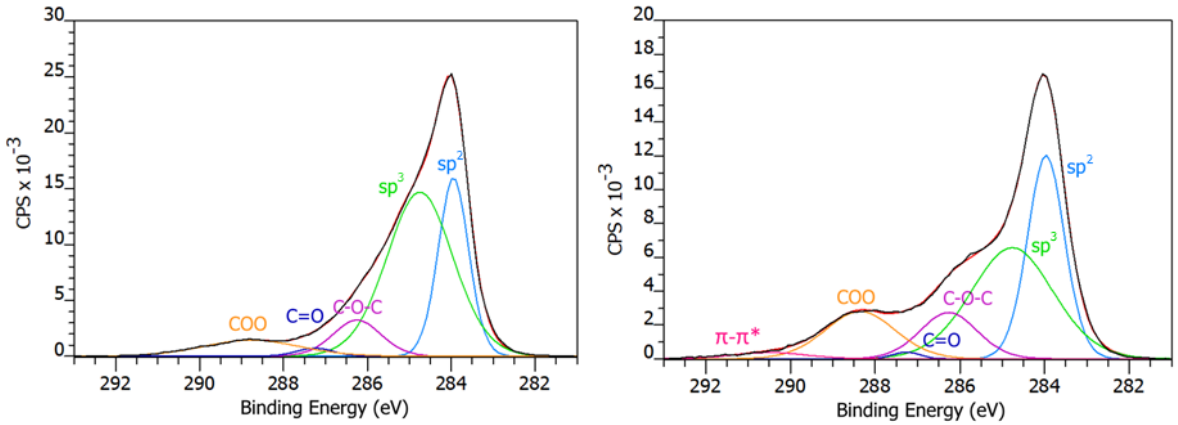

Figure 6 XPS spectra of the pristine (a), and O_2 plasma-treated (b) CF (P = 100 W, t = 5 min).

The C 1s peak of the pristine CF is fitted with 5 components. The two main substructures are assigned to C-C bonds where the C atom is either in sp^2 or sp^3 hybridation appearing respectively at binding energies (BE) of ~284 and 284.7 eV. Oxygenated components are identified at 286.3 eV: single bond C-O, mainly ethers and alcohols, 287.1 eV: double bond C=O such as ketones and aldehydes, and at ~289 eV: COO such as carboxylic acids [26,27]. The components FWHM was fitted at values between 1 to 2 eV; such broad FWHM implies that each component is composed of different subspecies, or these are included in slightly varying chemical environment. Yet, the resolution was not enough to precisely decompose these components into significant subspecies, especially the C-O-C component which could be composed of alcohol and ether functional groups, either aliphatic or aromatic due to the graphitic backbone of the CFs. The C 1s high resolution peak of O_2 plasma-modified CF

presents the same substructures plus another weak and wide component at 291.5 eV assigned the π-π* transition plasmons of the CF graphitic crystallites. The surface proportions of each substructure are reported in Table 2. As its relative area is low (≤ 1 %), the π-π* shake up is not taken into account in the following discussion and the other C 1s components contributions are recalculated without the π-π* influence.

Table 2 surface proportion of the C 1s components for untreated and O_2-plasma treated CFs under different powers (t = 5 min)

	sp^2 C (%)	sp^3 C (%)	C-O-C (%)	C=O (%)	COO (%)
Untreated CF	27.2 ± 1.4	54.8 ± 2.7	8.7 ± 0.5	1.5 ± 0.1	7.8 ± 0.4
50 W	33.4 ± 1.7	42.3 ± 2.1	7.0 ± 0.3	1.5 ± 0.1	15.8 ± 0.8
100 W	32.9 ± 1.6	40.0 ± 2.0	11.6 ± 0.6	0.8 ± 0.1	14.6 ± 0.7

Table 2 shows that when the CF is exposed to dioxygen plasma, (i) C-C bonds evolve in favor of the sp^2 carbons, as it increases from 27.2 to ≈ 33 %, while sp^3 carbon atoms' concentration decreases from 54.8 to ≈ 40 %; (ii) C-O-C slightly decreases for 50 W O_2 plasma from 8.7 to 7 %, and increases more significantly for 100 W, up to 11.6 %; (iii) C=O concentration remains low and even seems to decrease for 100 W, in favor of the COO component which shows the highest increase in proportion (7.8 for the untreated CF, up to 15.8 % for oxidized CF). This indicates that native surface sp^3 C atoms are more reactive and react with the activated oxidized species and form different oxidized functions. The increase in the sp^2 proportion implies that the graphitic carbons are less reactive towards the plasma and more chemically inert to the plasma functionalization. However, the XPS spectra do not allow to check a possible alteration of the graphitic crystalline structure. Furthermore, the plasma oxidation improves the surface chemistry, especially by only increasing the acidic component of the CF since the C=O concentration remains low indicating an efficient functionalization process. When the power is further increased, COO and C=O proportions do not increase. This could be explained either by a saturation effect of C=O and COO proportions or by the oxidation of remaining reactive sites in ether-like functional groups. In addition, volatile or non-adherent

compounds, such as CO_2 may be formed. Nevertheless, the global improvement of the CF surface chemistry explains the improvement of the SFE observed in Fig. 4, while possible chemical degradation competes with the functionalization in more drastic treatment conditions.

3.2 Dependence of the chemistry, morphology and crystallinity of modified CF on plasma conditions

The variation of the surface composition as reported here is however not as high as described in the literature [1,22,29]. The plasma efficiency, specifically O_2 plasma, may be improved by varying the reactive plasma densities for CF surface functionalization, as this plasma atmosphere induced the most important variations in the SFE components. The next graphs (Fig. 7) show the influence of the dioxygen plasma power, i.e. the electron and atomic oxygen densities, on the CF surface properties.

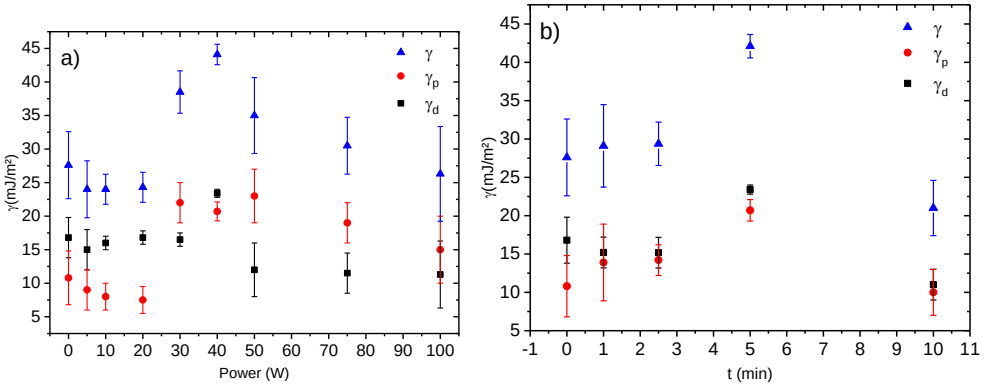

Figure 7 surface free energy (γ), its polar (γ_p) and dispersive (γ_d) components of CF treated in O_2 plasma a) for different applied powers (t = 5 min); b) for varying exposure time (P = 40 W).

Fig. 7a shows the dependence of the surface free energy and its components on the applied power for O_2 plasma. The SFE varies along 3 modes depending on the applied power: for power lower than 30 W, surface wettability is not improved as the SFE remains constant around the same value as measured for the untreated CF ($\gamma = 27 \pm 5$ mJ/m²). For intermediate power (30 to 50 W), SFE is significantly increased, as it almost doubled thanks to an increase in the polar component from around 10 mJ/m² to values around 21 mJ/m². The maximum SFE

(γ = 44 ± 1 mJ/m²) is measured for the optimal power of 40 W, with the corresponding dispersive and polar component values of respectively 23 ± 1 and 20 ± 1 mJ/m². Such an increase is related to the grafting of polar functions such as acid and ether groups detected in the XPS analysis above and less CF degradation. Then, the SFE decreases for higher power (> 50 W), to reach SFE values as low as 26 ± 7 mJ/m² for the applied power of 100 W.

A similar experiment was conducted for different exposure times at the optimal power of 40 W, these results are shown in Fig. 7b. In a same manner, 3 regimes are observed with no SFE improvement for short and long treatment times, respectively ≤ 2.5 min and > 5 min (SFE remains around 29 mJ/m²) and its increase for intermediate durations. Only the 5-min treatment led to the maximum value of SFE (γ = 44.1 ± 1 mJ/m²) close to the literature values [1,22,29]. For durations longer than 10 min, SFE is minimum at 21 ± 3 mJ/m². This dependence implies that in too smooth conditions, the functionalization is not sufficient and does not improve the CF surface properties. On the other hand, in too hard conditions, functionalization saturates quickly [32], and surface degradation by physical or chemical etching could impede the surface modification [17,27,28,33]. To verify the hypothesis of potential surface degradation, morphology and crystalline structure of the treated CF were checked. Fig. 8 shows the SEM images of untreated and plasma treated CF surfaces.

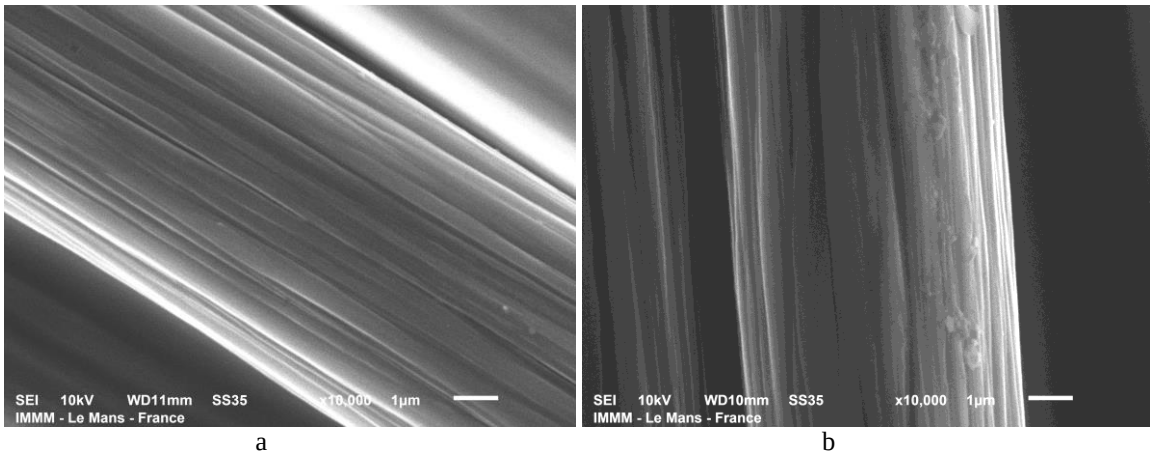

a b

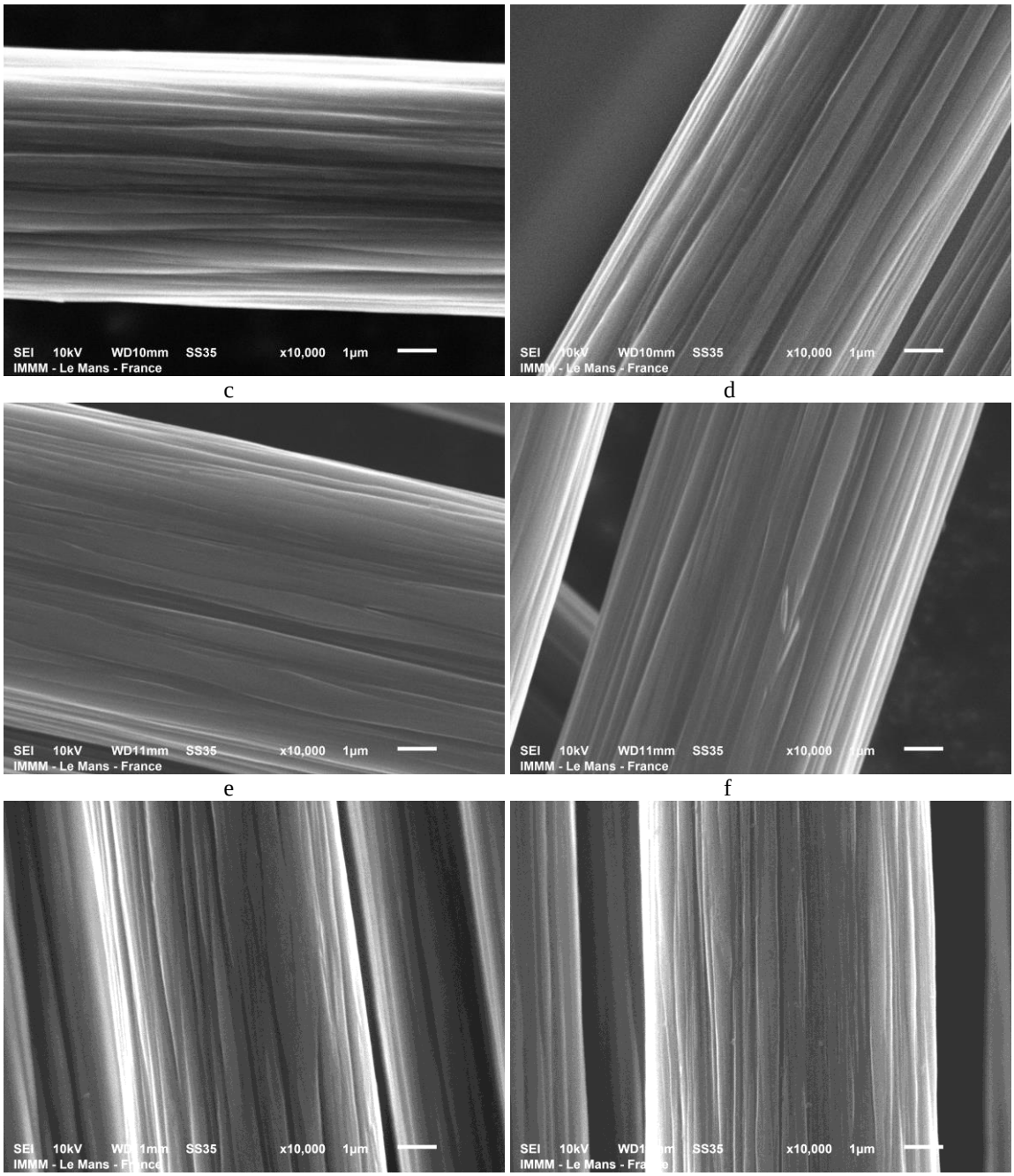

Figure 8 SEM pictures (magnification x10k) of T300 CF a) untreated, and plasma treated: b) Ar 100 W, 5 min; O_2 treated: c) 40 W, 1 min; d) 40 W, 10 min; e) 10 W, 5 min; f) 40 W, 5 min; g) 50 W, 5 min; h) 100 W, 5 min.

The morphology of the pristine fiber is characterized by linear trenches parallel to the fiber axis that induce some surface roughness (Fig. 8a). Oxidizing plasma-treatments (Fig. 8c-h) seem to retain the overall morphology and the roughness, as previously reported [10,11]. If ionic bombardment or chemical etching does occur, it is in a scale too low for inducing detectable changes in the morphology by SEM. The sole plasma condition: argon treatment for

at least 5 min at 100 W (Fig. 8b) induces surface alteration: small protrusions of several hundreds of nm appear on top of the linear structure over the length of the CF. In a general point of view, surface morphology modification seems to be limited and the initial structure present on untreated CF remains. While this roughness is beneficial for polymer matrices wetting and adhesion [10,11], the plasma treatment do not allow highlighting tremendous etching of the CF. In addition, the measured radius of the treated fiber remained close to that one for untreated fiber, around 6.7 ± 0.2 µm.

The high mechanical properties of composites are mostly controlled by matrix-fiber interfacial affinity and also on the mechanical properties of the so-called reinforced material, i.e. the carbon fiber. Therefore, the plasma treatment must not alter the crystalline structure and a Raman spectroscopy was performed to characterize the crystallinity of plasma-treated fiber (Fig. 9).

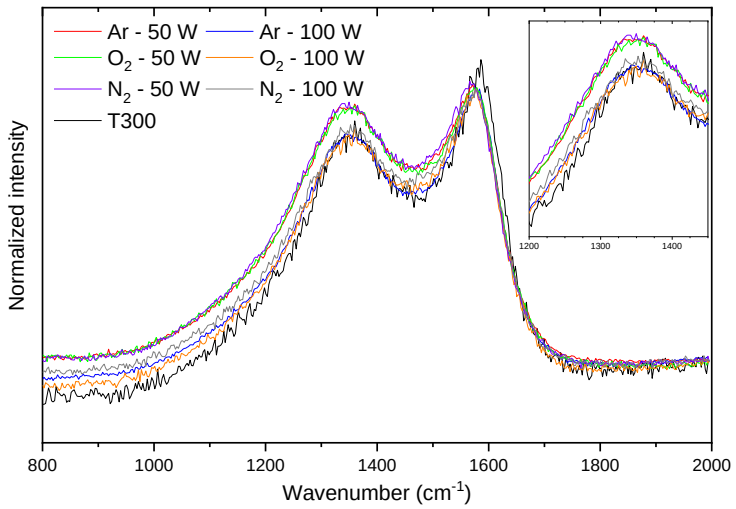

Figure 9 Raman spectra of CF: untreated (black) and plasma-treated for 5 min and for different powers (50 or 100 W) and different gas (Ar, N_2 and O_2).

Raman spectra of CF are composed of two main bands at 1350 cm^{-1} and 1575 cm^{-1} (Fig. 9) identified as respectively the D (for disorder) and the G (for graphitic) bands [33-36]. The D band is assigned to amorphous carbon vibrations while the G band is linked to the vibration of

carbon atoms included in graphitic planes. Their relative area and the shift of bands maxima depend on the proportion of sp^2 and sp^3 carbons in the sample depth and any modification of the orbital structure of carbon atoms will highlight potential functionalization [37-40]. Whatever the plasma-treatment, the G band shifts from 1575 cm^{-1} to value around 1565 cm^{-1} and its intensity is weakly decreasing. The bathochromic shift of the G band, while its intensity decreases shows that graphitic carbon is lost due to the plasma treatment. The shift, for limited crystalline alteration of the CF surfaces, is assigned to the amorphization of graphitic monocrystals and/or nanocrystals: the material evolves from local monocrystalline to polycrystalline structure [38]. The weak decrease of the G band intensity however indicates a weak increase in the sp^3 carbon sites, i.e. chemical defects due to the formation of a new bond under plasma-functionalization. This also implies that surface concentration of functional groups does not vary much with power or gas even if Raman spectroscopy in this spectral range is not well adapted for chemical group characterization.

At the same time, the D band intensity only increases for discharge power of 50 W and remains equal to that one of pristine sample for 100 W whatever the chemical nature of the atmosphere. The CF structure seems to be more sensitive to the electronic bombardment rather than the reactive species grafting and such behavior can be linked to an amorphization of the CF surface [38] probably induced by surface etching of some nanocrystal domains or size reduction.

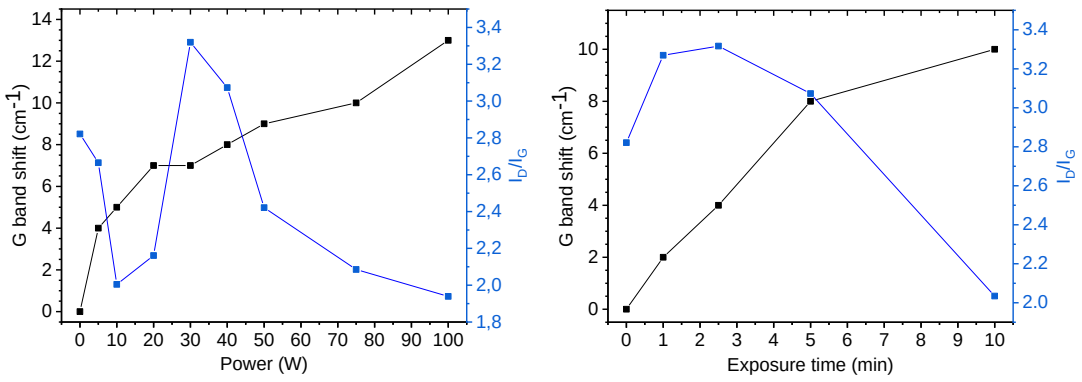

a) b)

Figure 10 Dependence of the G band shift (black) and the I_D/I_G area ratio on a) the applied power (t = 5 min); b) the exposure time (P = 40 W) for O_2 plasma-treated CF.

To highlight such modification of its crystalline structure, CF was treated in O_2 plasma at different powers and durations; the dependence of the associated G band shift and area ratio of the two bands is described in Fig. 10. Increasing the discharge power (Fig. 10a) or the duration (Fig. 10b) leads to a continuous increase of G band shift. This bathochromic shift reaches the value of 13 cm^{-1} for 100 W of applied power at fixed duration of 5 min and 10 cm^{-1} for 10 min of exposure with fixed power of 40 W. Furthermore, Fig. 10a shows a more complex variation of the I_D/I_G ratio with first a decrease (from 2.8 to 2.0 at $P \leq 20$ W), then a quick increase up to 3.3 at P = 30 W followed by a new decrease down to 2.0. Its dependence on duration (Fig. 10b) is more simple with a maximum value (= 3.3) for durations shorter than 2.5 - 3 min.

Even if numerous parameters influence the variation of G band shift and I_D/I_G ratio [38,40,41], some conclusions may be drawn. As the G band shift is mainly assigned to a decrease in the size of the graphitic crystalline domains, increasing the discharge power or the duration could induce a more and more pronounced surface degradation, such as chemical or physical etching. The more chaotic evolution of I_D/I_G is explained as follows: at low powers (Fig. 10a) the plasma is less chemically reactive and induces a more pronounced degradation of the amorphous phase related to the D band, while the graphitic phase is less altered. When the applied power increases, the increase of I_D/I_G is assigned to a modification of the balance in the sp^2 and sp^3 C atoms on the surface due to the plasma functionalization. Indeed, plasma modification breaks the sp^2 C backbone of the graphitic planes to graft heteroatoms (oxygen) and form functional groups, characterized by sp^3 bonds [3,38,40,41]. The D band increase gives evidence of the plasma functionalization. A too strong discharge power leads to a too reactive plasma and induces excessive oxidation of the CF surface shown by the I_D/I_G decrease,

removing both amorphous and crystalline structures as volatile oxidized compounds. Less resistant amorphous phase is removed, while the graphitic structure is altered and shifts to a polycrystalline phase shown by the G band shift. The duration (Fig. 10b) has a similar effect [22,40,41], where short time is not efficient for CF modification, and where too long duration enhances the plasma etching. These Raman results are coherent with those obtained on SFE dependence on power and duration on the SFE values (Fig. 4), demonstrating the narrow domain of plasma efficiency: below no effect of the plasma and beyond too strong effect inducing excessive CF alteration.

4. Conclusion

This study demonstrated the possible direct measure of SFE of plasma-treated CF. Such measurements are conducted by acquiring the wetting profiles of single CF strands immersed in different liquid probes. Solving the Young-Laplace equation allows to calculate the contact angles and thus, if polar and nonpolar liquids are used, to determine the surface free energies of plasma-treated CF. However, such measurement can only be accurate if several experimental precautions are considered. First, sampling probes have to be viscous to limit dynamic wetting of the surface. Second, high quality of the profile curve fitting has to be attained to keep as low as possible the CA values dispersion. This is critical as intrinsic high dispersions of the final SFE values are observed due to the variation of the geometrical properties of the different single strands, as well as to their varying morphological and physicochemical properties.

This study also showed that RF plasma-treatments induce alteration of the physicochemistry properties of CF and was highlighted by the SFE and corresponding static contact angles measures and calculations. The different tested gas showed however different efficiencies on the wettability of CF surface. Dioxygen showed the best result by increasing the CF surface energy (up to 44 mJ/m_2 for P = 40 W and t = 5 min) while altering its atomic

composition. More sensitive quantification of the surface functionality showed that dioxygen plasmas are the best candidate to increase the surface relative concentration of functional groups such as acidic (COO) and ether groups (C-O-C), which result in higher surface energy polar component. However, plasma-treatments showed a limited improvement of the surface properties, especially in the CF wettability behavior. While the surface topography modification remained low whatever the plasma treatment, either low efficiency plasma treatments, or excessive surface oxidation were observed if the power and duration are too low ($P < 30$ W at $t = 5$ min, $t > 2$ min with $P = 40$ W), or if both parameters are too high ($P > 50$ W at $t = 5$ min, $t > 5$ min with $P = 40$ W). Fine optimization of the plasma parameters is thus needed, especially in drastic conditions of plasma treatments, to avoid excessive surface functionalization. Indeed, these surface modifications have an impact on the CF crystalline properties, as shown by Raman spectroscopy. Nevertheless, such improvement of the surface wettability and surface chemistry, if finely controlled, improve the interfacial adhesion of the polymer matrix and the CF.

Acknowledgments

This study is part of the FORCE project supported by IRT Jules Verne (French Institute in Research and Technology in Advanced Manufacturing Technologies for Composite, Metallic and Hybrid Structures). The authors wish to associate the industrial and academic partners of this project; respectively Faurecia, Arkema, Mersen, PSA, Renault, Décathlon, DGA, CEA, Chantiers de l'Atlantique, CANOE.

5. References

[1] Tiwari S., Bijwe J. Surface treatment of carbon fibers - A review (2014) Procedia Technol. 14:505.

[2] Tiwari S., Sharma M., Panier S., Mutel B., Mitschang P., Bijwe J. Influence of cold remote nitrogen oxygen plasma treatment on carbon fabric and its composites with specialty polymers (2011) J. Mater. Sci. 46:964.

[3] Sharma M., Gao S., Mäder E., Sharma H., Wei L.Y., Bijwe J. Carbon fiber surfaces and

composite interphases (2014) Compos. Sci. Technol. 102:35.
[4] Cherif C., Textile materials for lightweight constructions, Springer Berlin Heidelberg, Berlin, Heidelberg, 2016.
[5] Yameen B., Álvarez M., Azzaroni O., Jonas U., Knoll W. Tailoring of poly(ether ether ketone) surface properties via surface-initiated atom transfer radical polymerization (2009) Langmuir. 25:6214–6220.
[6] Wavhal D.S., Fisher E.R. Hydrophilic modification of polyethersulfone membranes by low temperature plasma-induced graft polymerization (2002) J. Memb. Sci. 209:255.
[7] Kowbel W., Bruce C., Withers J.C., Ransone P.O. Effect of carbon fabric whiskerization on mechanical properties of C-C composites (1997) Compos. Part A Appl. Sci. Manuf. 28:993.
[8] Le Dû G., Celini N., Bergaya F., Poncin-Epaillard F. RF plasma-polymerization of acetylene: Correlation between plasma diagnostics and deposit characteristics (2007) Surf. Coatings Technol. 201:5815.
[9] Debarnot D., Mérian T., Poncin-Epaillard F. Film chemistry control and growth kinetics of pulsed plasma-polymerized aniline (2011) Plasma Chem. Plasma Process. 31:217.
[10] Kim J.-K., Mai Y.W. Engineered interfaces in fiber reinforced composites, Elsevier Sciences, 1998.
[11] Donnet J.B., Ehrburger P. Carbon fiber in polymer reinforcement (1977) Carbon 15:143.
[12] Novak R.C., Fracture in Graphite Filament Reinforced Epoxy Loaded in Shear, in: Compos. Mater. Test. Des., ASTM Inter. (1969) 540.
[13] McKee D.W. The copper-catalyzed oxidation of graphite (1970) Carbon 8:131.
[14] Yuan L.Y., Shyu S.S., Lai J.Y. Plasma surface treatments on carbon fibers. II. Mechanical property and interfacial shear strength (1991) J. Appl. Polym. Sci. 42:2525.
[15] Bascom W.D., Chen W.-J. Effect of plasma treatment on the adhesion of carbon fibers to thermoplastic polymers (1991) J. Adhes. 34:99.
[16] Garbassi F., Occhiello E., Surface plasma treatment, in: Lee S.M. (Ed.), Handb. Compos. Renf., VCH Publications, New York (1993) 625.
[17] Lee S.-W., Lee H.-Y., Jang S.-Y., Jo S., Lee H.-S., Choe W.-H., Lee S. Efficient preparation of carbon fibers using plasma assisted stabilization (2013),Carbon 55:361.
[18] Horie K., Hiromichi M., Mita I. Bonding of epoxy resin to graphite fibers (1976) Fiber Sci. Technol. 9:253.
[19] Dilsiz N. Plasma surface modification of carbon fibers: a review (2000) J. Adhes. Sci. Technol. 14:975.
[20] Raphael N., Namratha K., Chandrashekar B.N., Sadasivuni K.K., Ponnamma D., Smith A.S., Krishnaveni S., Cheng C., Byrappa K. Surface modification and grafting of carbon fibers: A route to better interface (2018) Prog. Cryst. Growth Charact. Mater. 64:75.
[21] Haye E., Busby Y., da Silva Pires M., Bocchese F.,Job N., Houssiau L., Pireaux J.J. Low-pressure plasma synthesis of Ni/C nanocatalysts from solid precursors: Influence of the plasma chemistry on the morphology and chemical state: (2018) ACS Appl. Nano Mater. 1:65.
[22] Li R., Ye L., Mai Y.-W. Application of plasma technologies in fibre-reinforced polymer composites: a review of recent developments (1997) Compos. Part A Appl. Sci. Manuf. 28:73.
[23] Jones F.R. A review of interphase formation and design in fibre-reinforced composites (2010) J. Adhes. Sci. Technol. 24:171.
[24] Owens D.K., Wendt R.C. Estimation of the surface free energy of polymers (1969) J. Appl. Polym. Sci. 13:1741.
[25] Aarts D.G.A.L., Van Der Wiel J.H., Lekkerkerker H.N.W. Interfacial dynamics and the

static profile near a single wall in a model colloid-polymer mixture (2003) J. Phys. Condens. Matter. 15:0953-8984.
[26] Briggs D., Beamson G., High Resolution XPS of Organic Polymers: The Scienta ESCA300 Database (Beamson, G.; Briggs, D.), (1993) J. Chem. Educ. 70:A25.
[27] Corujeira Gallo S., Charitidis C., Dong H. Surface functionalization of carbon fibers with active screen plasma (2017) J. Vac. Sci. Technol. A Vacuum, Surfaces, Film. 35:021404.
[28] Drzal L.T., Rich M.J., Lloyd P.F. Adhesion of graphite fibers to epoxy matrices: I. The role of fiber surface treatment (1983) J. Adhes. 16:1.
[29] Drzal L.T., Madhukar M. Fiber-matrix adhesion and its relationship to composite mechanical properties (1993) J. Mater. Sci. 28:569.
[30] Asset T., Job N., Busby Y., Crisci A., Martin V., Stergiopoulos V., Bonnaud C., Serov A., Atanassov P., Chattot R., Dubau L., Maillard F., Considerations to meet performance and stability requirements: (2018) ACS Catal., 8:893.
[31] Fitzer E., Weiss R. Effect of surface treatment and sizing of c-fibers on the mechanical properties of cfr thermosetting and thermoplastic polymers (1987) Carbon 25:455.
[32] Yang Z., Peng H., Wang W., Liu T. Crystallization behavior of poly(ε-caprolactone)/layered double hydroxide nanocomposites (2010) J. Appl. Polym. Sci. 116:2658.
[33] Jang J., Kim H. Improvement of carbon fiber/PEEK hybrid fabric composites using plasma treatment (1997) Polym. Compos. 18:125.
[34] Frank E., Steudle L.M., Ingildeev D., Sporl J.M., Buchmeiser M.R. Carbon fibers: Precursor systems, processing, structure, and properties (2014) Angew. Chemie - Int. Ed. 53:5262.
[35] Paris O., Zollfrank C., Zickler G.A. Decomposition and carbonisation of wood biopolymers - a microstructural study of soft wood pyrolysis (2005) Carbon 43:53.
[36] Snowdon M.R., Mohanty A.K., Misra M. study of carbonized lignin as an alternative to carbon black (2014) ACS Sustain. Chem. Eng. 2:1257.
[37] Byrne N., Setty M., Blight S., Tadros R., Ma Y., Sixt H., Hummel M. Cellulose-derived carbon fibers produced via a continuous carbonization process : Investigating precursor choice and carbonization conditions (2016) Macromol. Chem. Phys. 217:2517.
[38] Ferrari A., Robertson J. Interpretation of Raman spectra of disordered and amorphous carbon (2000) Phys. Rev. B - Condens. Matter Mater. Phys. 61:14095.
[39] Bernard S., Beyssac O., Benzerara K., Findling N., Tzvetkov G., Brown G.E. Raman and XRD study of anthracene-based cokes and saccharose-based chars submitted to high-temperature pyrolysis (2010) Carbon 48:2506.
[40] Bokobza L., Bruneel J.-L., Couzi M. Raman spectroscopy as a tool for the analysis of carbon-based materials (highly oriented pyrolitic graphite, multilayer graphene and multiwall carbon nanotubes) and of some of their elastomeric composites (2014) Vib. Spectrosc. 74:57.
[41] Vautard F., Ozcan S., Paulauskas F., Spruiell J.E., Meyer H., Lance M.J. Influence of the carbon fiber surface microstructure on the surface chemistry generated by a thermo-chemical surface treatment (2012) Appl. Surf. Sci. 261:473.